Oxygen K-Edge Emission and Absorption Spectroscopy of Iron Oxyhydroxide Nanoparticles

Benjamin Gilbert,[*] Christopher S. Kim,[†] Chung-Li Dong,[¶] Jinghua Guo,[¶] Peter S. Nico[*] and David K. Shuh[‡]

[*]*Earth Sciences Division, Lawrence Berkeley National Laboratory, 1 Cyclotron Road, Berkeley, CA 94720.*
[†]*Department of Physical Sciences, Chapman University, Orange, CA 92866.*
[¶]*Advanced Light Source, Lawrence Berkeley National Laboratory, 1 Cyclotron Road, Berkeley, CA 94720.*
[‡]*Chemical Sciences, Lawrence Berkeley National Laboratory, 1 Cyclotron Road, Berkeley, CA 94720.*

Abstract. Transition metal oxide and oxyhydroxide nanoparticles are the focus of considerable current interest in geochemistry. Much progress has been made in understanding the structure and phase relationships in mineral nanoparticles, but the effects of small size and modified surface structure on reactivity remains an outstanding problem. Common environmental nanoparticles have been shown to exhibit enhanced chemical reactivity relative to bulk mineral surfaces, but the origin of this behavior is not well established. We studied the electronic structure component of mineral reactivity by comparing soft x-ray absorption and emission spectra of bulk goethite (α-FeOOH) with spectra obtained from ~ 6 nm FeOOH nanoparticles and larger FeOOH nanoparticles obtained by hydrothermal coarsening. The semiconductor band gap is reduced in the FeOOH nanoparticles, mainly due to the presence of additional states in the upper valence band. We performed *ab initio* simulation of the electronic structure of oxygen sites at the 010 surface of goethite, and observe that oxygen sites with reduced metal coordination contribute to the O *2p* DOS at higher binding energy. Hence we conclude that FeOOH nanoparticle surfaces are more disordered than the surfaces of goethite, and that this structural component is likely the dominant cause of enhanced rates of reductive dissolution.

Keywords: iron oxyhydroxide, goethite, nanoparticles, x-ray absorption, x-ray emission, oxygen K-edge
PACS: 73.22.-f,78.70.Dm,78.70.En,91.67.-y

INTRODUCTION

Many low temperature abiotic and microbial geochemical processes cause the production of mineral nanoparticles in the environment [1]. These fine grain materials frequently play key roles in the transport of contaminants, the (photo)reductive degradation of organic molecules, and as electron acceptors or donors in microbial metabolism. However, despite observations of increased reactivity in nanoscale minerals [2, 3], there is little understanding of how small particle size affects the electronic properties and reactivity of environmentally relevant oxide nanoparticles. Thus, it is presently not possible to construct predictive models of nanoparticle roles in geochemical cycles, or to predict the environmental impact of man-made nanomaterials.

An important aspect of the reactivity of minerals is the electrochemical potential of the valence band (VB) and conduction band (CB) electrons [4]. One method of investigating absolute redox potentials of solution species is via electrochemical cells, as has been demonstrated for sulfide nanoparticles in non-aqueous solvents [5]. However, such methods are difficult for nanoparticles because slow diffusion rates to the electrode lead to very small currents that may be overwhelmed by electrode-bound species. Furthermore, the electrochemical measurement can drive redox reactions that can cause the appearance of unanticipated chemical species, requiring careful interpretation [6].

Recently it has been shown that the combination of x-ray absorption spectroscopy (XAS) and x-ray emission spectroscopy (XES) can determine the band gap and the absolute redox potential of electronic states in bulk iron and manganese oxide minerals [7]. The direct relationship between spectroscopic observations of semiconductor band energies and

electrochemical potential provides a predictive capability for the (photo)reduction dissolution of bulk mineral phases [8].

Combined XES/XAS spectroscopy is well suited to the study of nanoparticles and has provided the clearest verification of how quantum confinement separately affects the VB and CB of delocalized electron semiconductor nanoparticles [9]. In the present study, we used O K-edge XES/XAS to study the VB and CB of iron oxyhydroxide (FeOOH) nanoparticles, a common natural environmental nanoparticle [10], and a bulk goethite (α-FeOOH) reference.

EXPERIMENT

Iron oxyhydroxide nanoparticles approximately 6 nm in diameter were synthesized using the method of Guyodo et al. [11]. The nanoparticle size was determined by transmission electron microscopy (TEM) of dried nanoparticles and dynamic light scattering (DLS) measurements on aqueous suspensions at pH 5. Larger FeOOH nanoparticles were obtained by hydrothermally coarsening the as-synthesized material in water at pH 5.5 and 90 ˚C for a number of days [12]. A mineral specimen of bulk goethite (α-FeOOH) was provided by G. A. Waychunas.

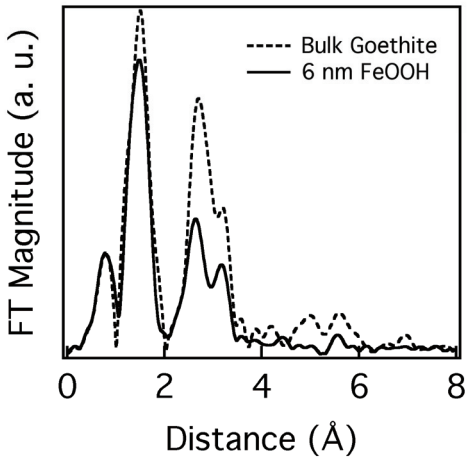

FIGURE 1. The coordination environment of Fe atoms in bulk goethite (α-FeOOH) and ~ 6 nm diameter FeOOH nanoparticles, obtained from the Fourier transform of Fe K-edge EXAFS data. The interatomic distance is not corrected for phase shifts associated with photoelectron scattering.

The crystal phase of the nanoparticles was investigated by x-ray diffraction (XRD) and extended x-ray absorption fine structure (EXAFS) spectroscopy at the Fe K-edge. The XRD data exhibited considerable peak broadening caused both by small crystallite size and the presence of structural disorder, making phase identification challenging [12]. EXAFS data were acquired in transmission mode from dried powders mixed in BN held between Kapton windows.

X-ray absorption and non-resonant emission spectroscopy was acquired at the oxygen K-edge from dried powders pressed into indium metal. The beamline energy calibration was verified with a sample of NiO. The beamline resolution was 0.2 eV for XAS and 0.5 eV for XES; the fluorescence spectrum was collected with an excitation energy of 530 eV and a resolution of 0.3 eV. We verified that the electronic band gap of bulk goethite, identified as the energy gap between the inflection points of the VB and CB edges, agreed with previously reported value (2.5 eV; ref. 7).

Spin polarized multiple scattering calculations of the density of states of goethite were performed with the FEFF 8.2 code [13]. The structure of goethite, including the magnetic ordering, was obtained from ref. 14.

RESULTS

Figure 1 compares the site averaged local coordination geometry of iron in bulk goethite and in FeOOH nanoparticles, obtained from the Fourier transform of the k^3-weighted EXAFS signal (2 – 14.6 $Å^{-1}$). The EXAFS radial distribution function (RDF) from the nanoparticles decreases more rapidly with interatomic distance than for the bulk goethite reference, but is otherwise similar. Quantitative fitting of the first shell (not shown) revealed that the mean Fe-O bond distance in the nanoparticle sample matches the bulk to within 0.03 Å. The static disorder in the FeO_6 octahedra is slightly greater in the nanoparticles, with the Debye-Waller disorder parameter found to be $\sigma^2_{nano} = 0.01$ Å^2 *vs.* $\sigma^2_{bulk} = 0.096$ Å^2.

X-ray absorption and emission spectroscopy at the oxygen K-edge show that the VB and CB states at the electronic band gap are modified in the nanoparticles relative to bulk goethite (Fig. 2). The emission data show that the VB is broader in the nanoparticles, and as a consequence the onset of the VB lies ~ 0.35 eV higher in energy than for bulk goethite. The absorption data reveal that the onset of the CB is ~ 0.15 eV lower in energy in the nanoparticles, and exhibit more complex lineshape differences.

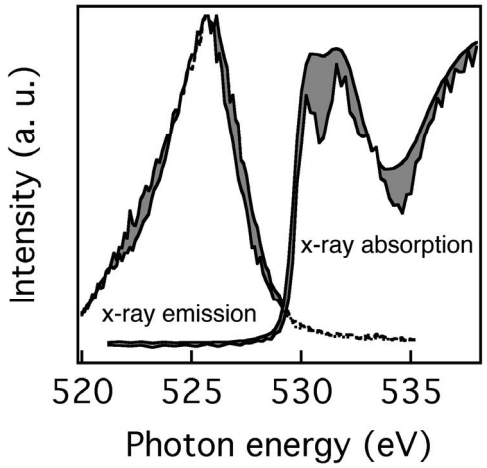

FIGURE 2. Soft x-ray emission and absorption spectra from bulk goethite (lower curves) and ~ 6 nm FeOOH nanoparticles (upper curves) at the oxygen K-edge. The difference between bulk and nanoparticle spectra is shaded grey.

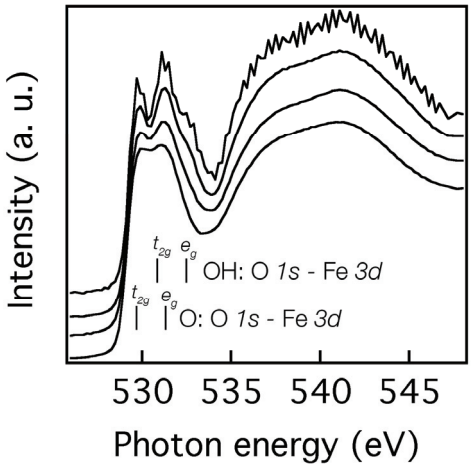

FIGURE 3. Oxygen K-edge absorption spectra of ~ 6 nm FeOOH nanoparticles as a function of hydrothermal coarsening time. From the bottom curve: 0 days coarsening, 1 day and 8 days. The top spectrum is from bulk goethite.

An expanded view of the x-ray absorption spectra of the as-synthesized nanoparticles is given in Fig. 3, and compared with data from larger particles and the bulk reference.

DISCUSSION

Electronic Structure Changes

Conduction Band

Oxygen K-edge absorption spectroscopy of iron oxides has been studied experimentally and theoretically by many groups [15–17]. The oxygen K-edge XAS is sensitive to the unoccupied *p*-weighted density of states (*p*DOS) due to the $\Delta l = \pm 1$ dipole selection rule for photoabsorption. Because the Fe-O bond is partially covalent, O *2p* states hybridize with Fe *3d* orbitals and hence the lowest energy (pre-threshold) fine structure is associated with ligand to metal charge transfer excitations [18, 19]. Thus, O K-edge XAS are sensitive to metal atom coordination geometry and *3d* occupation (oxidation state).

The ferric iron sites in bulk goethite are situated within distorted octahedral sites and adopt a high spin configuration. Relative to O K-edge XAS of bulk hematite (α-Fe_2O_3) [7], the pre-threshold region of bulk goethite exhibits additional peaks that are due to the presence of two non-equivalent oxygen sites (oxygen ions and hydroxide groups). It has been verified by x-ray photoelectron spectroscopy (XPS) that the O *1s* core level in the hydroxide groups is chemically shifted by 1.2 eV to higher binding energy relative to oxygen sites [20]. This shifts the energy positions of XAS features from the two sites even though the photoabsorption process involves ligand transitions to the same iron site. The dominant contributions to the oxygen pre-threshold XAS are tentatively indicated in Fig. 3, where unoccupied Fe *3d* states are labeled with the assumption of ideal O_h geometry.

A notable feature of the nanoparticle XAS is the apparent absence of the pre-threshold contributions from hydroxide sites. As shown in Figs. 2 and 3, there are only two resolvable contributions and the full pre-threshold structure evolves as the particle size is increased. However, the proportion of hydroxide group oxygen atoms in FeOOH nanoparticles is expected to be greater than in the bulk when the larger surface area is considered. Thus, we infer the presence of a mechanism that reduces the relative chemical shift of O *1s* core level in FeOOH oxygen and hydroxide sites.

Figure 3 also shows that the pre-threshold peaks are broader in the nanoparticles, and sharpen with increasing particle size. We interpret the broader peaks to indicate the presence of numerous distinct, distorted iron sites in the nanoparticles. While the FeO_6 octahedra are considerably distorted in bulk goethite, all iron sites are equivalent. Simple peak fitting indicates that the mean peak positions (i.e., the ligand field splitting of the unoccupied *3d* states) is slightly reduced in the nanoparticles.

Valence Band

Oxygen K-edge emission spectra show an enhancement of the lower and upper VB DOS in

FeOOH nanoparticles relative to goethite. *Ab initio* cluster calculations have shown that the upper VB is associated with Fe *3d* – O *2p* bonds [18], with Fe-OH and non-bonding O *2p* states lying at lower energies. This DOS enhancement may be partially related to the broadening of Fe *3d* derived states that is attributed to structural disorder. However, it is clear that additional VB DOS states are present in the nanoparticles. We hypothesize that these states are associated with the nanoparticle surface.

While certain synthesis methods can manufacture highly crystalline facetted nanoparticles, low temperature precipitation processes more often produce spheroidal particles with no apparent facets [11, 12]. Although iron sites at the surface of hydrated ferric iron minerals are usually fully coordinated [22], the coordination of surface oxygen sites can be significantly lower than the bulk. We tested the effects of reduced oxygen coordination on O *2p* DOS in FeOOH by simulating the electronic structure of sites at the (010) cleavage face of goethite. As shown in Fig. 4, oxygen atoms with fewer than the three iron neighbors contribute *2p* DOS intensity at higher energy.

We conclude that the O K-edge XES and the simulation are consistent with a greater number of under-coordinated oxygen sites on the surfaces of FeOOH nanoparticles relative to the surfaces of goethite.

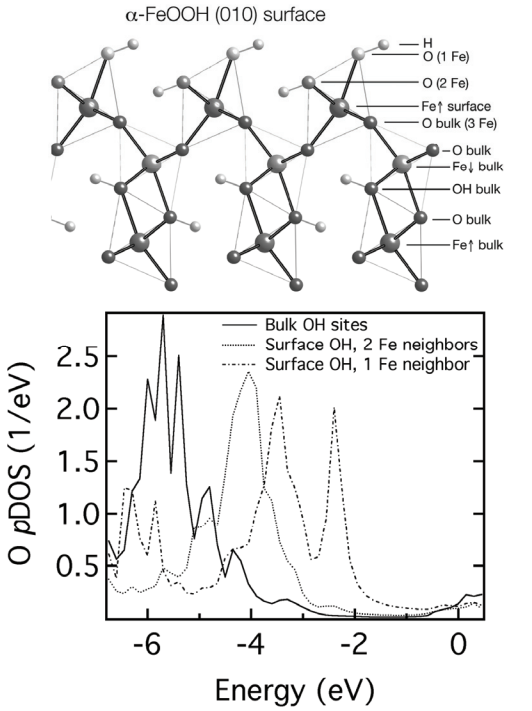

FIGURE 4. FEFF multiple scattering calculations of the *p*-weighted density of states (DOS) for oxygen atoms in three distinct hydroxide sites at the goethite 010 surface. The sites are displayed in the crystal model, and differ in the number of iron neighbors. The calculations show that surface O *2p* states are less tightly bound than states in the bulk.

Implications for Reactivity

Here we discuss the implications of the observed spectroscopic data on the redox reactivity of FeOOH nanoparticles. Redox reactions at the water-mineral interface involve charge transfer processes either between mineral and adsorbate (mineral as reagent), or between surface bound reagents (mineral as catalyst) [4, 23, 24]. The absolute energy positions of the electronic states in the mineral relative to the adsorbate determine whether such processes are possible [8]. However no quantitative predictions can be made concerning the rates of possible reactions, which depend on the molecular details of the interfacial charge transfer process [24].

A key observation is that the band gap in FeOOH nanoparticles is reduced relative to bulk goethite, with two implications for photochemical processes. First, a greater proportion of sunlight can be absorbed by FeOOH nanoparticles, creating VB holes and CB electrons that may drive subsequent redox chemistry. However, because the VB band edge lies at higher energy, the oxidizing power of VB holes is lowered. While the reducing power of CB electrons is less affected, photooxidation is frequently the more efficient process at the surfaces of illuminated iron oxide minerals [25].

The reductive dissolution of ferric iron minerals is an important component of the iron cycle and a feature of the metabolism of certain bacteria in anoxic environments [23, 26]. Because our data indicate that the CB states in FeOOH nanoparticles are not greatly modified relative to bulk goethite, we do not anticipate changes in the ability of aqueous reductants, including bacterial electron transfer molecules, to use FeOOH nanoparticles as electron acceptors.

However, our data suggest that there may be structural reasons for enhanced rates of reductive dissolution observed in FeOOH nanoparticles [2]. The free energy of the reductive dissolution of ferric iron includes contributions from both the charge transfer step and the formation of free aqueous ferrous iron. The presence of structural disorder and the reduced coordination of surface oxygen sites are consistent with a lower surface

Fe-O bond strength. Therefore, we suggest that structural rather than electronic contributions to nanoparticle reactivity may dominate for processes involving mineral dissolution.

CONCLUSIONS

Combined XAS/XES spectroscopy provides a relatively direct measurement of the energy positions of valence and conduction band states in semiconductor minerals and thus is well suited for investigations of band edge modifications in nanoparticles. Relative to bulk goethite, 6 nm FeOOH nanoparticles exhibit broadening of CB Fe *3d* derived states, and VB enhancement at the band edge. We conclude that these changes are caused by structural disorder, especially the presence of under-coordinated oxygen sites at the nanoparticle surface.

ACKNOWLEDGMENTS

Financial support for this work came from the Director, Office of Science, of the U.S. Department of Energy under Contract No. DE-AC02-05CH11231. Iron K-edge EXAFS spectra were acquired on beamline 10-2 at the Stanford Synchrotron Radiation Laboratory (SSRL). Oxygen K-edge absorption and emission spectra were acquired at beamline 7.0.1 at the Advanced Light Source (ALS). The SSRL is operated by Stanford University on behalf of the U.S. Department of Energy (DOE), Office of Basic Energy Sciences (OBES). The ALS is supported by the Director, Office of Science, OBES, of the U.S. DOE under Contract No. DE-AC02-05CH11231.

REFERENCES

1. B. Gilbert and J. F. Banfield, *Rev. Mineral. Geochem.* **59**, 109-155 (2005).
2. A. J. Anschutz and R. L. Penn, *Geochem. Trans.* **6**, 60-66 (2005).
3. A. S. Madden and M. F. Hochella, Jr., *Geochim. Cosmochim. Acta* **69**, 389-398 (2005).
4. G. E. Brown, Jr., *et al*., *Chem. Rev.* 99, 77-174 (1999).
5. E. Kucur, J. Riegler, G. A. Urban and T. Nann, *J. Chem. Phys.* 119, 2333-2337 (2003).
6. K. J. McKenzie and F. Marken, *Pure Appl. Chem.* **73**, 1885-1894 (2001).
7. D. M. Sherman, *Geochim. Cosmochim. Acta* **69**, 3249-3255 (2005).
8. Y. Xu and M. A. Schoonen, *Am. Mineral*. 85, 543-556 (2000).
9. J. Lüning, J. Rockenberger, S. Eisbitt, J. E. Rubensson, A. Karl, A. Kornowski, H. Weller and W. Eberhardt, *Solid State Commun* **112**, 5-9 (1999).
10. C. van der Zee, D. R. Roberts , D. G. Rancourt, and C. P. Slomp, *Geology* **31**, 993-996 (2003).
11. Y. Guyodo, A. Mostrom, R. L. Penn and S. K. Banerjee. *Geophys. Res Lett.* **30**, 1512 (2003).
12. G. A. Waychunas, C. S. Kim and J. F. Banfield, *J. Nanoparticle Res.* **7**, 409-433 (2005).
13. A.L. Ankudinov, B. Ravel, J.J. Rehr, and S.D. Conradson, *Phys. Rev. B* **58**, 7565 (1998).
14. J. B. Forsyth, I. G. Hedley and C. E. Johnson, *J. Phys. C* **1**, 179-188 (1968).
15. F. M. F. de Groot, M. Grioni, J. C. Fuggle, J. Ghijsen, G. A. Sawatzky, and H. Petersen, *Phys. Rev. B* **40**, 5715 (1989).
16. J. van Elp and A. Tanaka, *Phys. Rev. B* **60**, 5331-5339 (1999).
17. Z. Y. Wu, S. Gota, F. Jollet, M. Pollak, and M. Gautier-Soyer and C. R. Natoli, *Phys. Rev. B* **55**, 2570-2577 (1997).
18. D. M. Sherman, *Phys. Chem. Minerals* **12**, 161-175 (1985).
19. D. M. Sherman and T. D. Waite, *Am. Mineral.* **70**, 1262-1269 (1985).
20. I. D. Welsh and P. M. A. Sherwood, *Phys. Rev. B* **40**, 6386 (1989).
21. P. A. van Aken, B. Leibscher and V. J. Styrsa, *Phys. Chem. Mineral.* **25**, 494-498 (1998).
22. T. P. Trainor, A. M. Chaka, P. J. Eng, M. Newville, G. A. Waychunas, J. G. Catalano, and G. E. Brown, *Surface Science*, **573**, 204-224 (2005).
23. W. Stumm and B. Sulzberger, *Geochim. Cosmochim. Acta* **56**, 3233-3257 (1992).
24. A. G. Stack, K. M. Rosso, D. M. A Smith and C M. Eggleston, *J. Colloid Interf. Sci.* **274**, 442-450 (2004).
25. S. O. Pehkonen, R. L Seifert and M. F. Hoffman, *Environ. Sci. Technol.* **29**, 1215-1222 (1995).
26. D. R. Lovely, *Ann Rev Microbiol* 47:263-290 (1993).